Kasetsart J. (Nat. Sci.) 49 : 626 - 638 (2015)

Direct Adaptive Input Shaping Using On-Line Frequency Domain Information and Extremum-Seeking Optimization

Withit Chatlatanagulchai[1,*], Sermsak Chotana[1] and Chonlawit Prutthapong[2]

ABSTRACT

The input shaping technique convolves the reference command with a properly designed impulse sequence, creating a shaped reference command that avoids exciting the under-damped vibratory system to achieve zero residual vibration on a point-to-point maneuver. The input shaper needs to know the natural frequencies and damping ratios of the vibratory system to design such an impulse sequence. When system configurations change, the natural frequencies and damping ratios also change, and the input shaper must be updated with this new information. In this paper, a point-by-point discrete Fourier transform (DFT) algorithm was used to compute the frequency content of the vibratory signal. The identified natural frequencies were directly updated into the input shaper. Extremum-seeking optimization was used to further adjust the damping ratios for minimal vibration. The proposed technique was applied to a flexible-link robot manipulator. The manipulator was commanded to have a point-to-point maneuver with changing payload. The experimental results, based on cases with or without DFT and extremum seeking, showed that with the proposed technique, minimum residual vibration was obtained even when the payload changed, without having to know the amount of payload.

Keywords: adaptive input shaping, extremum seeking, frequency domain, flexible link robot

INTRODUCTION

Input shaping techniques reduce the residual vibration in under-damped systems by convolving the input to the systems with a sequence of impulses (Smith, 1957; Singer and Seering, 1990). The impulses' amplitudes and timings are optimally designed such that the shaped input avoids exciting the damped natural frequencies of the under-damped systems.

Numerous applications have been reported using the techniques. Recent applications include: increasing the swing of a wrecking ball (Maleki and Singhose, 2013); reducing the motion-induced oscillation in a category of aerial lifts commonly called cherrypickers (Hongxia *et al.*, 2012); preventing unwanted noise and vibration in an automotive wiper system (Zolfagharian *et al.*, 2013); rejecting vibration in a beam-type solar cell substrate transport robot (Park *et al.*, 2012); controlling sloshing in a cylindrical container (Hamaguchi and Taniguchi, 2012); reducing vibration of the flexible appendage of a planar space robot (Kasai and Kojima, 2012); and reducing the swing of helicopter sling load (Park *et al.*, 2012).

1 Department of Mechanical Engineering, Faculty of Engineering, Kasetsart University, Bangkok 10900, Thailand.

2 Julajomklao Navy Dockyard, The Royal Thai Naval Dockyard Headquarter, Royal Thai Navy, Samut Prakan 10290, Thailand.

* Corresponding author, e-mail: fengwtc@ku.ac.th

Received date : 17/10/13 Accepted date : 03/02/15

The input shaping techniques require the systems' natural frequencies and damping ratios to compute the impulse sequence. Therefore, the accuracy of this information is vital to the performance of the techniques.

More impulses have been added to the impulse sequence to reduce the sensitivity of the vibration to the natural frequency and damping ratio variations (Vaughan *et al*., 2008) at the expense of longer delay in the reference command.

Several adaptive techniques in the time domain have been proposed to identify the systems' natural frequencies and damping ratios on-line (Bodson, 1998; Cutforth and Pao, 2004; Kozak *et al*., 2004; Rhim and Book, 2004; Park *et al*., 2006; Stergiopoulos and Tzes, 2007; Pereira *et al*., 2012; Cole and Wongratanaphisan, 2013). Some of their drawbacks are: 1) the system mathematical model is required and must be linear; 2) the techniques require persistent excitation of the inputs; 3) the adaptive algorithm requires high computational time; and 4) the systems need to have repetitive maneuvers.

Only a few adaptive techniques in the frequency domain exist in the literature. Tzes and Yurkovich (1993) and Yurkovich *et al*. (1989) applied a real-time version of a frequency domain system identification method called empirical transfer function estimation contained in Ljung (1987) to estimate plant natural frequencies. Their technique is based on assumptions of the actual plant being linear and a smooth function of frequencies. Only natural frequencies, not damping ratios, can be adapted with this technique.

Compared to the time-domain system identification methods, the frequency-domain methods converge faster, are relatively insensitive to noise and do not suffer from over or under parameterization (Tzes and Yurkovich, 1991).

The current study proposed a novel adaptive input shaping technique. A point-by-point discrete Fourier transform (DFT) algorithm was used to find the frequency content in the vibratory signal in real time. This on-line frequency domain information was then used to determine the plant's natural frequencies. Having been fed the real-time plant's natural frequencies, the input shaper can be redesigned to match with the ever changing system. The system's damping ratios—another important parameter in designing the input shaper—are difficult to find even via the frequency domain information. In the current technique, the damping ratios were adapted on-line based on extremum-seeking optimization to minimize the vibratory signal magnitude. The extremum-seeking optimization (Ariyur and Krstic, 2003; Zhang and Ordonez, 2012) can obtain a local minimum of the cost function without having to know the gradient; therefore, the plant's mathematical model is not required.

This proposed technique is simple and practical and has several advantages over the past works: 1) the technique can adapt the input shaper to time-varying systems, whose natural frequencies and damping ratios continuously change; 2) the technique does not depend on the accuracy of the plant's mathematical model. In fact, the mathematical model is not used in this technique. Being a model-independent technique, it can then be naturally applied to more complicated or nonlinear systems; 3) the technique uses the frequency-domain information, which is relatively less sensitive to noise than that of the time domain; 4) the technique adapts multiple parameters so both the system natural frequencies and damping ratios of all vibratory modes can be simultaneously adapted by the extremum-seeking algorithm for minimum-possible residual vibration; 5) the technique does not require persistent excitation of inputs; 6) the technique does not require repetitive maneuvers; and 7) the technique is readily applicable to a new system without having to determine the new system's natural frequencies and damping ratios off-line.

The proposed technique was applied to the point-to-point movement of a flexible-link robot manipulator whose payload varied with time.

MATERIALS AND METHODS

In this section, the basics of discrete Fourier transform, input shaping and extremum seeking are separately explained, followed by the overall configuration of the proposed technique.

Discrete Fourier transform

The discrete Fourier transform (DFT) of a finite-length sequence $x(n)$ of length N, that is, $0 \le n \le N-1$, is given by Equation 1:

$$X(k) = \sum_{n=0}^{N-1} x(n) e^{-j\left(\frac{2\pi kn}{N}\right)}, \; k = 0, 1, ..., N-1. \quad (1)$$

The Fourier transform of $x(n)$ is given by Equation 2:

$$X(\omega) = \sum_{n=0}^{N-1} x(n) e^{-j\omega n}, \quad (2)$$

The discrete Fourier transform $X(k)$ corresponds to the sampled $X(\omega)$ at the uniformly spaced frequencies $\omega = 2\pi k / N$.

Therefore, the DFT can be used to find the frequency content in a signal, with several advantages: 1) the correspondence between $x(n)$ and $X(k)$ is one-to-one; 2) an extremely fast computer algorithm—the so-called fast Fourier transform (FFT)—is available to compute the DFT; and 3) the DFT is appropriate for digital computer realization because it is discrete and of finite length in both the time and frequency domains.

Input shaping

Figure 1 shows the input shaping for a flexible system where $\bar{r}$ is the original reference input, normally a step signal. The switch is for the user to select whether to use the input shaper or not. The input shaper is a cascade of FIR filters; each filter handles one vibratory mode. The shaped reference input, which is the output of the input shaper, is given to the flexible system to follow. The flexible system can be open-loop or closed-loop with known natural frequencies and damping ratios. Suppose the flexible system has p finite vibratory modes, then it can be written as Equation 3:

$$P = \prod_{j=1}^{p} \frac{\omega_{nj}^2}{s^2 + 2\zeta_j \omega_{nj} s + \omega_{nj}^2}, \quad (3)$$

where s is the Laplace transform operator, ω_{nj} are the j th-mode natural frequencies and ζ_j are the j th-mode damping ratios. y is the system output.

The input shaper is in the form of Equation 4:

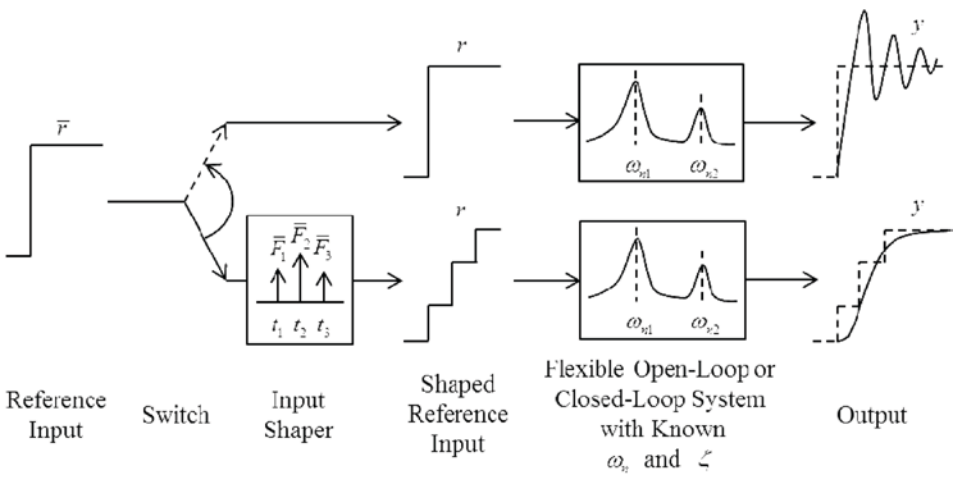

Figure 1 Input shaping for a flexible system, where $\bar{r}$ is the reference input, r is the shaped reference input, $\bar{F}_i$ are the impulse amplitudes, t_i are the impulse time locations, ω_n is the natural frequency, ζ is the damping ratio and y is the system output.

$$F(z)=\prod_{i=1}^{m}F_i(z), \tag{4}$$

where m is the number of vibratory modes in consideration,

$$F_i(z)=\left(\bar{F}_{i1}+\bar{F}_{i2}z^{-round\left(\frac{t_{i2}}{t_s}\right)}+\bar{F}_{i3}z^{-round\left(\frac{t_{i3}}{t_s}\right)}\right),$$

$$\bar{F}_{i1}=1/\left(1+2K_i+K_i^2\right),$$

$$\bar{F}_{i2}=2K_i/\left(1+2K_i+K_i^2\right),$$

$$\bar{F}_{i3}=K_i^2/\left(1+2K_i+K_i^2\right),$$

$$K_i=e^{\frac{-\zeta_i\pi}{\sqrt{1-\zeta_i^2}}},\ t_{i2}=\frac{\pi}{\omega_{ni}\sqrt{1-\zeta_i^2}},\ t_{i3}=\frac{2\pi}{\omega_{ni}\sqrt{1-\zeta_i^2}},$$

t_s is the sampling time, and z is the z-transform operator.

Note that the three-impulse version of the input shaper is used. The first two impulses are designed such that their impulse responses cancel each other for zero vibration. If the first impulse applies at time zero, the unknowns are then the time and magnitude of the second impulse. With the knowledge of the natural frequency and damping ratio of the system, the unknowns can be found in closed form by setting the impulse responses to zero. The third impulse is obtained from setting derivatives of the impulse responses, with respect to the natural frequency and damping ratio, to zero. Therefore, having the third impulse reduces the sensitivity to parameter changes providing more robustness (Vaughan *et al*., 2008).

Note that the powers of z in the FIR filter must be negative integers. Therefore, *round* (.) is used to round the real numbers to nearest integers. This approximation results from the fact that the input shaper is designed in continuous time, whereas its implementation is in discrete time. To avoid this approximation, a digital input shaping filter was presented in Murphy and Watanabe (1992).

More details on the derivation of the input shaping equations above can be found in Chatlatanagulchai and Saeheng (2009) and Chatlatanagulchai *et al*. (2009).

Perturbation-based extremum seeking algorithm

A perturbation-based extremum seeking algorithm, whose diagram is shown in Figure 2, was implemented and requires finding x to minimize $y = f(x)$. The algorithm tracks the function output in response to a small sinusoidal perturbation with a frequency ω, to move it in the down-hill direction without computing the function's gradient; therefore, the method does not require a mathematical model.

Using a high-pass filter with a cut-off frequency around ω and a low-pass filter with a cut-off frequency around 2ω, it was shown in

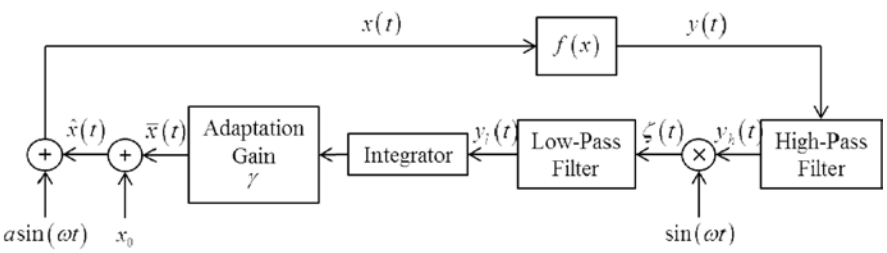

Figure 2 Perturbation-based extremum seeking, where $x(t)$ is the independent signal, $f(x)$ is the function to be minimized, $y(t)$ is the minimized signal, $y_h(t)$ is the signal from the high-pass filter, ω is the designed frequency, $\zeta(t)$ is the signal to the low-pass filter, $y_l(t)$ is the signal from the low-pass filter, γ is the adaptation gain, $\bar{x}(t)$ is the signal after multiplying the adaptation gain, x_0 is the bias signal, $\hat{x}(t)$ is the signal after bias and a is the amplitude of the sine wave

Ariyur and Krstic (2003) that an algorithm in Figure 2 leads to Equation 5:

$$\dot{\tilde{x}} \approx \frac{a\gamma f''\left(x^*\right)}{2}\tilde{x}, \quad (5)$$

where x^* is a minimum point of f, $\hat{x}$ is the estimation of x^*, and $\tilde{x} = \hat{x} - x^*$. In the minimization problem, if $a > 0$ and $\gamma > 0$, $\tilde{x}$ will approach zero asymptotically.

Overall configuration of the proposed technique

Figure 3 shows the overall configuration of the proposed technique.

The extremum seeking finds an estimated damping ratio $\hat{\zeta}$ of the true damping ratio ζ to minimize the residual vibration $\hat{a}$. The magnitude of $\hat{a}$ is quantified from the vibratory signal a. There are several choices for this quantification; this study used a quantity given by Equation 6:

$$\hat{a} = \int |a| dt, \quad (6)$$

where the integration is taken over the preceding movement of the plant. From the extremum seeking diagram in Figure 2, y is $\hat{a}$, x is $\hat{\zeta}$, and $f(x)$ is the parts of the system contained in the dashed box in Figure 3.

The point-by-point DFT computes the frequency content of a. To maintain the constant length N of the data sequence, when a new data point of a becomes available, the oldest data in the sequence is erased. The point-by-point DFT gives out an estimated flexible plant's natural frequency $\bar{\omega}_n$. With the known feedback controller, the estimated closed-loop natural frequency $\hat{\omega}_n$ can be calculated of the true natural frequency ω_n.

The input shaper then receives updated estimates of ω_n and ζ and uses them to redesign the impulse sequence.

RESULTS

Flexible-link robot system

The flexible-link robot hardware used in the experiments is shown in Figure 4. A two-feet steel ruler was used as the flexible link and the adjustable payload was placed at its tip. Two accelerometers were attached at the tip and in the middle. A strain gauge was placed near the pivot

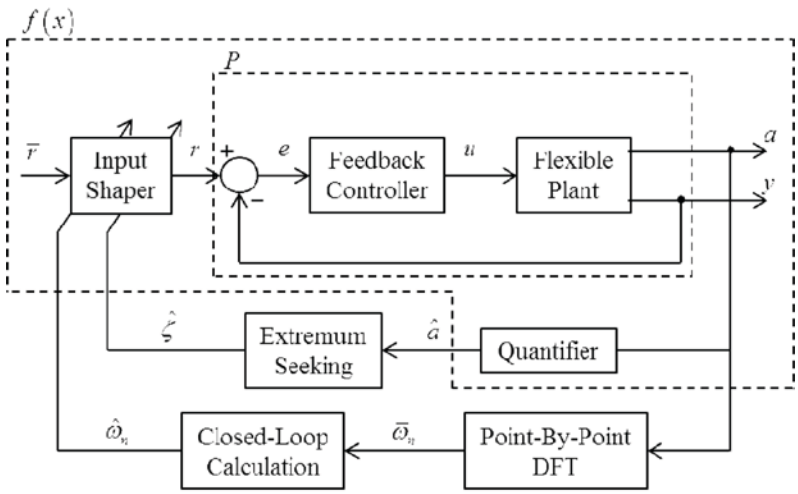

Figure 3 Overall configuration of the proposed technique. The overall system has a feedback controller to make the output y follow the shaped reference input r closely, where a is a vibratory signal, relating to the magnitude of the residual vibration $\hat{a}$. Usually a is obtained from vibration sensors such as accelerometer. P is the closed-loop system with natural frequency ω_n and damping ratio ζ.

point. An optical encoder was used to measure the angle of the direct current motor. The payloads were two packs of 10 small denomination silver coins with each pack weighing approximately 75 g.

The schematic diagram of the flexible-link robot, together with its experimental setup, is given in Figure 5,

For the experimental setup, a data acquisition board was put in the target computer, which was connected to the host computer via a personal computer (PC)-to-PC local area network. Both computers were running the Labview software (version 2010; National Instruments; Austin,TX, USA) and its pertinent module and toolboxes. The tip and middle accelerometers sent acceleration signals to the analog input channels. The strain gauge signal was connected with a quarter-bridge strain gauge circuit, whose output

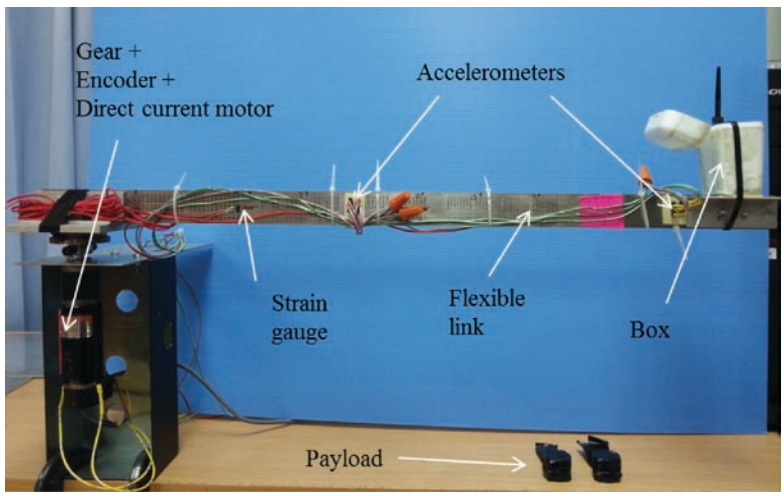

Figure 4 Flexible-link robot hardware used in our experiments.

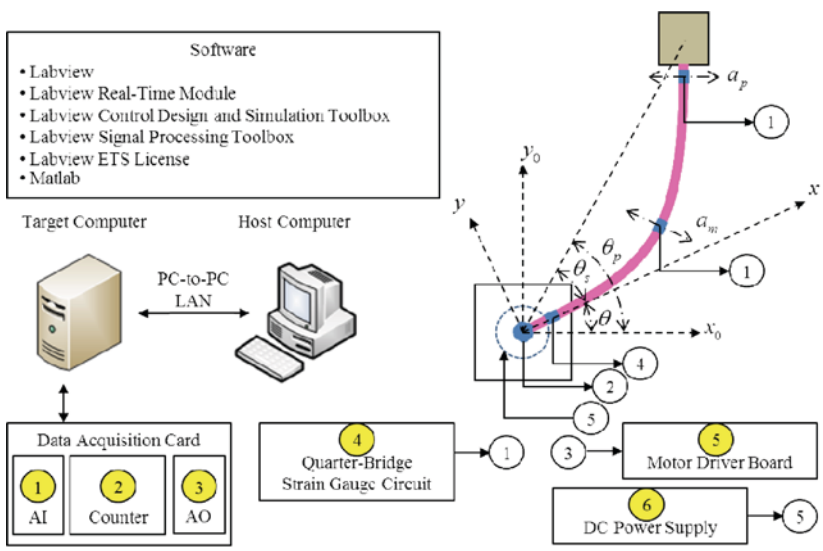

Figure 5 Schematic diagram of the flexible-link robot and its experimental setup, where θ is the motor rotational angle; θ_s is additional angle of the payload as obtained from the strain gauge; $\theta_p = \theta + \theta_s$ is the payload angle; a_p is the payload acceleration, measured from the tip accelerometer; and a_m is the mid-section acceleration, measured from the middle accelerometer.

voltage was connected to the analog input channel. The optical encoder measured the motor angular position. Its signal was connected to the counter channel and the control effort u was sent to the motor driver from the analog output channel. A direct current power supply powered the motor driver board.

Applying the proposed technique to the flexible-link robot

Figure 6 shows the application of the proposed technique to the flexible-link robot.

Because the flexible-link robot has infinitely many modes, the closed-loop system P is given by Equation 7:

$$P = \prod_{j=1}^{\infty} \frac{\omega_{nj}^2}{s^2 + 2\zeta_j \omega_{nj} s + \omega_{nj}^2}. \qquad (7)$$

From the off-line frequency contents of the payload acceleration a_p and middle acceleration a_m signals, the first and second modes make the greatest contribution. It appeared that a_p seemed to identify the first mode well, while a_m showed more of the second mode. Therefore, $\hat{a}_p$ was used to identify ζ_1, while $\hat{a}_m$ was used to identify ζ_2. Similarly, a_p was used to identify ω_{n1}, while a_m was used to identify ω_{n2}.

The PI controller's gains are $k_p = 0.1$ and $k_i = 0.05$.

Within the extremum seeking, the following design parameters were used: $\omega = 2$ rad.s^{-1}; a high-pass filter $s / (s + h)$, where $h = 1$; a low-pass filter $l / (s + l)$, where $l = 2$; $a_{\zeta_1} = 0.0001$ and $a_{\zeta_2} = 0.00015$ are amplitudes of the sine functions in the algorithm; $\gamma_{\zeta_1} = -0.007$ and $\gamma_{\zeta_2} = -0.01$ are the adaptation gains.

The initial values of $\hat{\omega}_{n1}$, $\hat{\omega}_{n2}$, $\hat{\zeta}_1$, and $\hat{\zeta}_2$ were 9 rad.s^{-1}, 70 rad.s^{-1}, 0.017, and 0.019, respectively.

The point-by-point DFT uses 3,000 data points. Since a_p was used to identify ω_{n1}, a possible range from 4 to 14 rad.s^{-1} was chosen. The maximum frequency content magnitude of a_p must take place at a frequency within this possible range and must be larger than an upper limit of 7 for $\hat{\omega}_{n1}$ to get updated with the new frequency value. Similarly, a possible range for a_m to identify ω_{n2} is from 50 to 105 rad.s^{-1} with an upper limit of 10.

The objective was to have the payload angle θ_p track the reference $\bar{\theta}_r$ as closely as possible with minimum residual vibration and amidst payload changes.

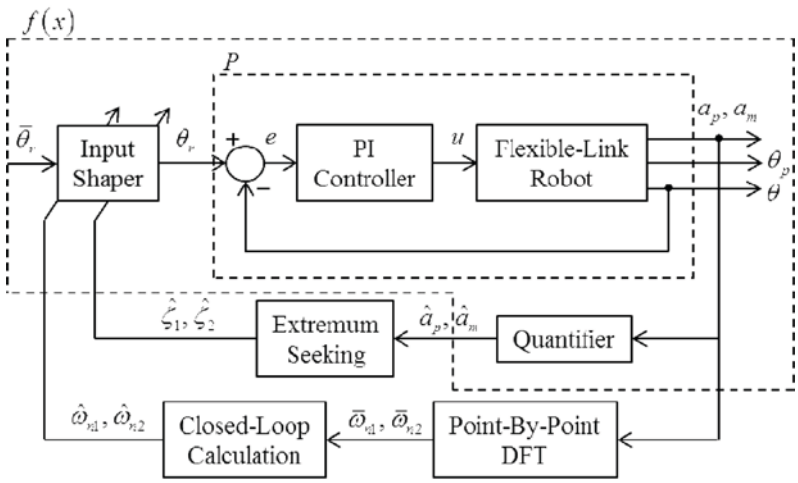

Figure 6 The proposed technique applied to the flexible-link robot where $\bar{\theta}_r$ is the motor reference angle, θ_r is the motor shaped reference angle, and e is the motor angle tracking error. Other variables are as previously defined in Figure 3 and 5.

Experimental results

A square-wave reference, $\bar{\theta}_r$, of 30 degrees amplitude and 20 seconds period was used. The payload was changed from 0 to 20 coins (1 coin weighs approximately ?? g) at the 0 s, then from 20 to 10 coins at 100 s, then from 10 to 0 coins at 200 s, then from 0 to 20 coins at 300 s—all during maneuvers.

Three experimental cases were compared: 1) basic input shaping (I); 2) input shaping with DFT (I-D); and 3) input shaping with DFT and extremum seeking (I-D-E). The results of the unshaped case are not shown, but the vibration was far worse than in the three cases.

In the proposed I-D-E case, a new natural frequency $\hat{\omega}_{n1}$ for the first mode was obtained whenever the maximum frequency content magnitude of the payload acceleration a_p, $\left|A_p(\omega)\right|_{\max}$, occurred at a frequency within a window from 4 to 14 rad.s^{-1} and was larger than 7. Obtaining a new natural frequency $\hat{\omega}_{n2}$ for the second mode was similar, but the middle acceleration a_m was used with a window from 50 to 105 rad.s^{-1} and an upper magnitude limit of 10. Figure 7 compares the time progressions of $\left|A_p(\omega)\right|$ and $\left|A_m(\omega)\right|$ between the two cases: I and I-D-E. Figures 7a and 7b contain $\left|A_p(\omega)\right|$ and $\left|A_m(\omega)\right|$ in the I case, respectively. Figures 7c and 7d contain $\left|A_p(\omega)\right|$ and $\left|A_m(\omega)\right|$ in the I-D-E case, respectively.

For clarity, Figure 8 presents the same information as that of Figure 7 but in a two-dimensional view.

Figure 9 shows the adaptations of natural frequencies and damping ratios used by the input shaper in the I-D-E case. Figures 9a and 9b are the first-mode natural frequency and damping ratio, respectively. Figures 9c and 9d are the second-mode natural frequency and damping ratio, respectively.

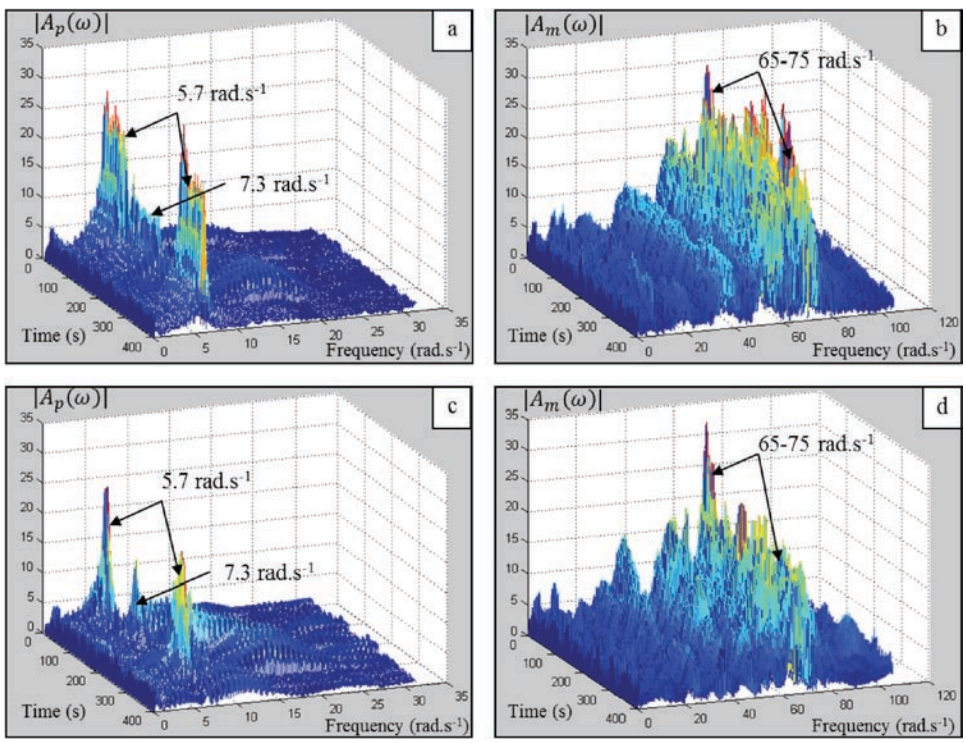

Figure 7 Discrete Fourier transform magnitude of: a) the payload acceleration signal in the I case; b) the middle acceleration signal in the I case; c) the payload acceleration signal in the I-D-E case; and d) the middle acceleration signal in the I-D-E case.

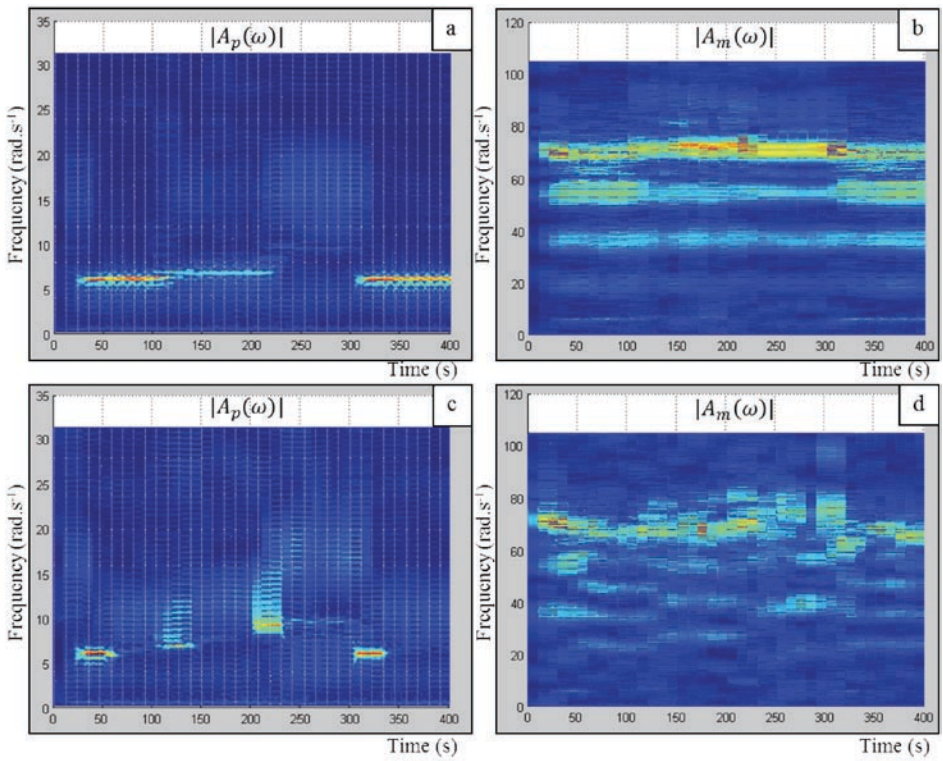

Figure 8 Discrete Fourier transform magnitude in 2-dimensional view: a) the payload acceleration signal in the I case; b) the middle acceleration signal in the I case; c) the payload acceleration signal in the I-D-E case; and d) the middle acceleration signal in the I-D-E case.

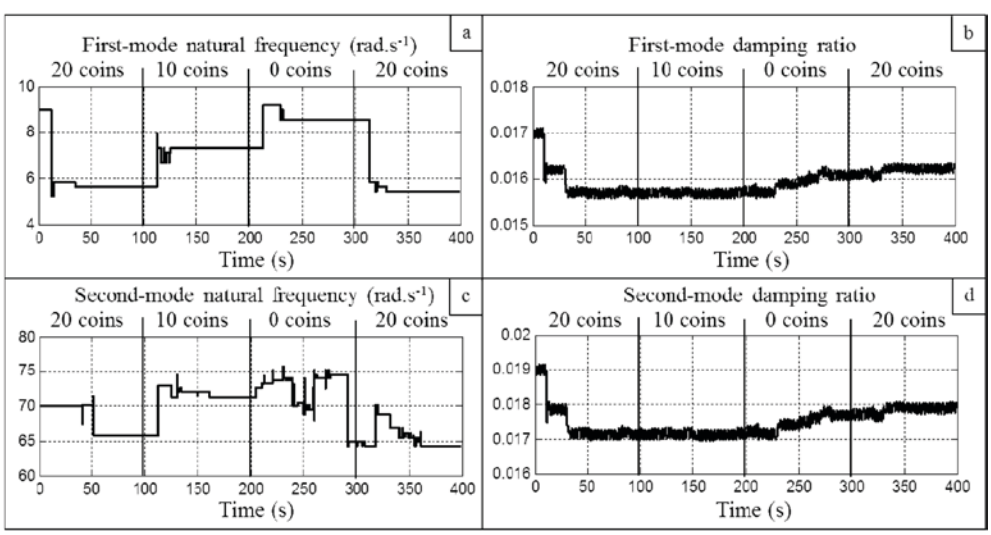

Figure 9 Adaptations of natural frequencies and damping ratios used by the input shaper in the I-D-E case: a) First-mode natural frequency; b) First-mode damping ratio; c) Second-mode natural frequency; d) Second-mode damping ratio. (Low denomination silver coins were used as the payload with each coin weighing approximately 75 g.)

Figure 10 contains a comparison of the accumulated payload vibration, $\hat{a}_p$, given in among the three cases: a) input shaping + DFT + extremum seeking (I-D-E); b) input shaping + DFT (I-D); and c) input shaping (I).

Figure 11 contains a zoom-in picture of the payload angular position θ_p and its reference square wave. Figure 11a belongs to the I-D-E case, and Figure 11b belongs to the I case.

DISCUSSION

Figures 7a and 7b show higher levels of the frequency content of the acceleration signals in the input shaping only case when compared with those of the proposed I-D-E case in Figures 7c and 7d. Since the frequency content is proportional to the signal energy in the time domain, a higher level means more vibration. The I-D-E technique was able to reduce the frequency content because when the payload changed, the natural frequencies of the system changed, the I-D-E technique detected a new peak in frequency content and updated the input shaper with the new natural frequency information. Once the input shaper was updated with the new natural frequency, it suppressed that natural frequency, resulting in a lower peak and less vibration.

Figure 8c (the top view of Figure 7c) shows that when the payload was 20 coins, the first-mode natural frequency was approximately 5.7 rad.s^{-1}, when the payload was 10 coins, it was approximately 7.3 rad.s^{-1}, and when there is no payload, it is around 8.5 rad.s^{-1}. By comparing

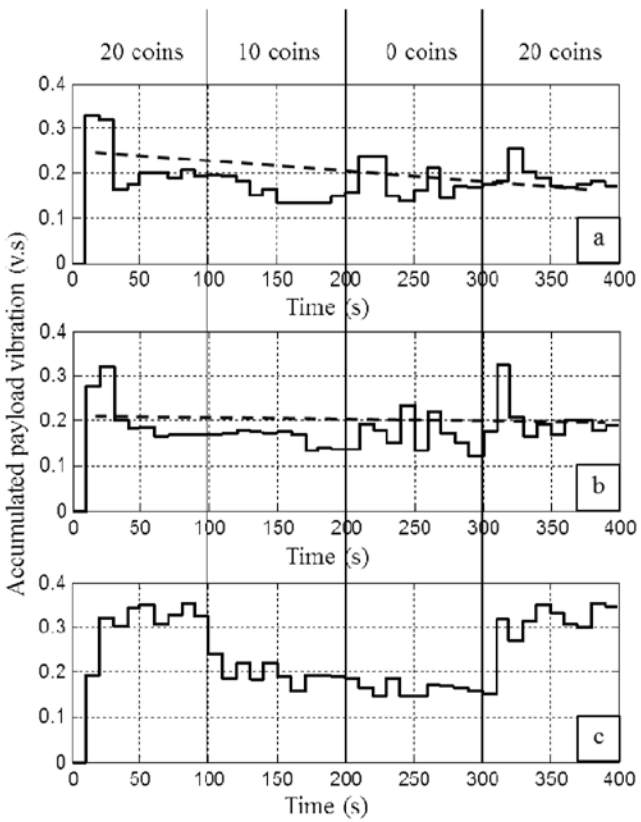

Figure 10 Comparison of the accumulated payload vibration, $\hat{a}_p$, among the three cases: a) input shaping + DFT + extremum seeking (I-D-E); b) input shaping + DFT (I-D); and c) input shaping (I). (Low denomination silver coins were used as the payload with each coin weighing approximately 75 g.)

Figure 8c with Figure 8a, it can be seen that the I-D-E technique quickly attenuated the frequency content peaks. Note that in the I case of Figure 8a, the frequency content peaks at approximately 8.5 rad.s^{-1} and seemed to attenuate well because the initial value $\hat{\omega}_{n1} = 9$ rad.s^{-1} was used by the input shaper and was unchanged through the experiment.

From Figures 8b and 8d, the second-mode natural frequency is in the range 65–75 rad.s^{-1}. Similarly, the I-D-E technique was able to suppress the frequency content peak of the second-mode, even though the result was not as obvious as that of the first mode.

Figures 9a and 9c show that when the payload changes, the natural frequencies change and the I-D-E technique obtains updated natural frequencies from the frequency content of the acceleration signals and sends them to the input shaper. The second-mode natural frequency fluctuated more than that of the first-mode due to the greater fluctuation in the acceleration signal obtained from the middle accelerometer. However, they both followed the same trend. Figures 9b and 9d show that the first-mode and second-mode damping ratios are adapted by the extremum seeking to minimize the accumulated payload vibration $\hat{a}_p$, given in . It should be noted that they are adapted in the same way because the same input ($\hat{a}_p$) is used in both damping ratios.

A comparison of Figures 10a and 10c shows that the I-D-E technique reduced the accumulated payload vibration from 0.3 to 0.2 (or 33%) when the payload was 20 coins and from 0.2 to 0.15 (or 25%) when the payload was 10 coins. However when the payload was 0 coins, the vibration was not reduced much because, in the I case, the fixed input shaper was designed from a natural frequency close to that of the 0 coin case.

Comparing Figures 10a and 10b, it is evident that extremum seeking helped to reduce the overall vibration as can be seen from the two dashed lines presenting the trend of the vibration. The trend of the vibration of the I-D-E case showed more of a decrease than that of the I-D case.

The study objective was to have the payload angular position track its reference square wave trajectory as closely as possible with minimum residual vibration. Comparing Figures 11a and 11b, showing the 20-coin payload, it can be seen that the payload angular position followed its reference very well in the I-D-E case. The settling time in the I-D-E case reduced from 10.5 s in the I case to 1.5 s—a settling time reduction of around 85%.

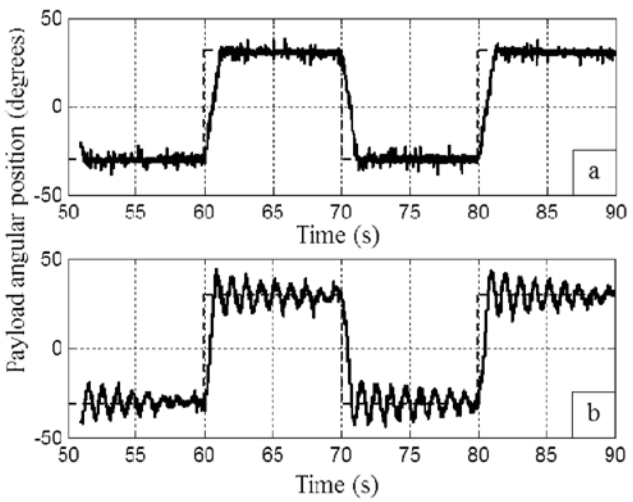

Figure 11 Comparison of the payload angular position, θ_p (deg.): a) the I-D-E case and b) the I case. The dashed lines are reference trajectories.

CONCLUSION

An adaptive input shaping technique was presented. The system's natural frequencies used by the input shaper were adapted in real time by evaluating the frequency content of the vibratory signals. The system's damping ratios were gradually adapted by extremum seeking for minimum vibration.

The proposed adaptive input shaping technique can be applied to time-varying systems or complicated systems, whose natural frequencies and damping ratios are difficult to find. The technique does not require a mathematical model or *a priori* information of the natural frequencies and damping ratios to operate. It can also be applied to a different system without much offline redesign.

Suggested future studies include replacing the extremum seeking with a more elaborate or intelligent optimization algorithm such as swarm optimization and applying the technique to more complicated or actual engineering systems.

LITERATURE CITED

Ariyur, K.B. and M. Krstic. 2003. **Real-Time Optimization by Extremum-Seeking Control.** 1st ed. Wiley Interscience. Hoboken, NJ, USA. 236 pp.

Bodson, M. 1998. An adaptive algorithm for the tuning of two input shaping methods. **Automatica** 34: 771–776.

Chatlatanagulchai, W. and K. Saeheng. 2009. Real-time reference position shaping to reduce vibration in slewing of a very-flexible-joint robot. **J. Res. Eng. Tech.** 6: 51–66.

Chatlatanagulchai, W., T. Srivongsa and P.H. Meckl. 2009. Reference input shaping to reduce move time of a very flexible one-link manipulator. **Kasetsart J. (Nat. Sci.)** 43: 411–421.

Cole, M.O.T. and T. Wongratanaphisan. 2013. A direct method of adaptive FIR input shaping for motion control with zero residual vibration. **IEEE/ASME Trans. on Mechatronics** 18: 316–327.

Cutforth, C.F. and L.Y. Pao. 2004. Adaptive input shaping for maneuvering flexible structures. **Automatica** 40: 685–693.

Hamaguchi, M. and T. Taniguchi. 2012. Damping control of liquid container with swing-type active vibration reducer on mobile robot by using inverse model of sloshing. **Trans. Jap. Soc. of Mech. Eng. C** 78: 2106–2120.

Hongxia, J., Z. Fumin and J. Vaughan. 2012. Using input shaping to repress two-mode residual vibration on aerial lifts, pp. 667–671. *In* **Proceeding Int. Conf. on Control, Automation and Systems.** IEEE. NY, New York, USA.

Kasai, S. and H. Kojima. 2012. Input-shaped link motion control of planar space robot equipped with flexible appendage. **Trans. Jap. Soc. Aeronaut. Space Sci.** 55: 205–213.

Kozak, K., I. Ebert-Uphoff and W. Singhose. 2004. Locally linearized dynamic analysis of parallel manipulators and application of input shaping to reduce vibrations. **ASME J. Mech. Design** 126: 156–168.

Ljung, L. 1987. **System Identification Theory for the User.** 1st ed. Prentice Hall. Englewood Cliffs, NJ, USA. 609 pp.

Maleki, E. and W. Singhose. 2013. Maximizing the swing of a human-operated wrecking ball, pp. 112–117. *In* **Proceeding Int. Conf. on Industrial Technology.** IEEE. New York, Ny, USA.

Murphy, B.R. and I. Watanabe. 1992. Digital shaping filters for reducing machine vibration. **IEEE Trans. Robot. Autom** 8: 285–289.

Park, C.H., D.I. Park and T.K. Yoon. 2012. Identification of flexible mode and motion simulation for beam type solar cell substrate transport robot, pp. 1181–1184. *In* **Proceeding Int. Conf. on Control, Automation and Systems.** IEEE. New York, NY, USA.

Park, J., P.H. Chang, H.S. Park and E. Lee. 2006.

Design of learning input shaping technique for residual vibration suppression in an industrial robot. **IEEE/ASME Trans. Mechat.** 11: 55–65.

Pereira, E., J.R. Trapero, I.M. Diaz and V. Feliu. 2012. Adaptive input shaping for single-link flexible manipulators using an algebraic identification. **Control Eng. Pract.** 20: 138–147.

Rhim, S. and W.J. Book. 2004. Adaptive time-delay command shaping filter for flexible manipulator control. **IEEE/ASME Trans. Mechat.** 9: 619–626.

Singer, N.C. and W.C. Seering. 1990. Preshaping command inputs to reduce system vibration. **ASME J. Dyn. Syst., Meas. Control** 112: 76–82.

Smith, O.J.M. 1957. Posicast control of damped oscillatory systems. **Proc. IRE.** 45: 1249–1255.

Stergiopoulos, J. and A. Tzes. 2007. Adaptive input shaping for nonlinear systems: A case study. **ASME J. Dyn. Syst., Meas. Cont.** 129: 219–223.

Tzes, A. and S. Yurkovich. 1991. Application and comparison of on-line identification methods for flexible manipulator control. **Int. J. Robot. Res.** 10: 515–527.

Tzes, A. and S. Yurkovich. 1993. An adaptive input shaping control scheme for vibration suppression in slewing flexible structures. **IEEE Trans. Cont. Syst. Tech.** 1: 114–121.

Vaughan, J., A. Yano and W. Singhose. 2008. Comparison of robust input shapers. **J. Sound Vibr.** 315: 797–815.

Yurkovich, S., F.E. Pacheco and A.P. Tzes. 1989. On-line frequency domain information for control of a flexible-link robot with varying payload. **IEEE Trans. Autom. Cont.** 34: 1300–1304.

Zhang, C. and R. Ordonez. 2012. **Extremum-Seeking Control and Applications** (1st ed.). Springer. London, UK. 197 pp.

Zolfagharian, A., A. Noshadi, M.Z. Zain and A.R. Bakar. 2013. Practical multi-objective controller for preventing noise and vibration in an automobile wiper system. **Swarm Evol. Comput.** 8: 54–68.